AAS 14-376

RENDEZVOUS AND PROXIMITY OPERATIONS AT THE EARTH-MOON L2 LAGRANGE POINT: NAVIGATION ANALYSIS FOR PRELIMINARY TRAJECTORY DESIGN

Kuljit Mand[*], David Woffinden[†], Pol Spanos[‡] and Renato Zanetti[§]

The Earth-Moon L2 point has attracted considerable attention as a potential location for future missions that enable spacecraft to explore beyond the far-side of the Moon and other deep space celestial bodies. The capability to rendezvous and dock is required for multiple mission objectives. A critical element associated with the trajectory design is determining the navigation requirements, which are indirectly affected by operating in this new environment.

Three preliminary trajectory designs are proposed that employ a newly developed relative targeting algorithm that accounts for multi-body affects at L2. The trajectory designs range from replicating traditional rendezvous profiles to introducing strategies that capitalize on the unique relative motion at L2. Navigation requirements necessary for rendezvous and docking at L2 are then derived and validated for each trajectory. These requirements are subsequently utilized for a sensor suite analysis to identify an optimal sensor suite for each trajectory within a quick and automated framework.

INTRODUCTION

NASA's manned space program and the aerospace community are shifting focus from low Earth orbit (LEO) back to deep space. In particular, the Earth-Moon L2 Lagrange point, referred to here simply as L2, has become a potential location for spacecraft such as a space station or propellent depot. This can be completed as a relatively short term goal and act as a precursor to farther destinations.

Numerous reasons exist to place a spacecraft in this region. The L2 point, along with L1, is part of an Interplanetary Superhighway System, allowing travel by low energy pathways and greatly decreasing propulsion costs for deep space travel.[1] It is an optimal location for refueling as it is nearly at Earth escape energy.[2] Additionally, because of its location behind the Moon, a spacecraft orbiting near the L2 point can either be placed within a radio quiet zone, for radio astronomy,[3] or act as a communications satellite for exploration and colonization based on the far-side of the Moon.[4]

Significant work has been conducted for transfer trajectories to various Lagrange points such as the Earth-Moon L2 location,[5,6] L2 halo orbit determination and insertion,[7,8,9] as well as for station keeping and formation flying.[10] However, research related to rendezvous and close proximity operations while in the vicinity of the Lagrange points, particularly the L2 point, is lacking. In particular, one critical element is identifying a navigation system that can properly support close proximity operations at L2.

For deep space exploration, rendezvous and docking serve as a critical capability to satisfy basic mission objectives. These operations become necessary for assembling larger units in orbit, re-supplying and refueling, exchanging crew, repairing spacecraft, or rejoining an orbiting vehicle with a lander or other auxiliary vehicle.[11]

[*] Graduate Student, Mechanical Engineering and Materials Science, Rice University, kuljitmand@gmail.com
[†] Senior Member of the Technical Staff, Charles Stark Draper Laboratory, dwoffinden@draper.com
[‡] Lewis B. Ryon Professor of Mechanical Engineering and Materials Science, Rice University, spanos@rice.edu
[§] Senior Member of the Technical Staff, Charles Stark Draper Laboratory, rzanetti@draper.com

The trajectory design for rendezvous and docking at the L2 environment is necessary in order to support missions at this location, yet the relative motion experienced during standard rendezvous operations in LEO is different from the relative motion at L2. Consequently, the rendezvous techniques developed over the last half century must be re-evaluated and adjusted. The trajectory design and on-orbit operations must take into account an assortment of random disturbances that introduce deviations to a desired path.

The conventional approach to model trajectories influenced by random, or stochastic, processes can involve heavily computational and time consuming Monte Carlo simulations. However, an alternative method exists to model the dispersion and navigation error in the preliminary design stages of a rendezvous trajectory, known as linear covariance analysis (LinCov). LinCov can greatly decrease the time required to evaluate multiple trajectories and the complex interaction of the guidance, navigation and control (GN&C) system, and find an optimal solution. Once the design is complete, the linearization assumptions inherent with the covariance propagation can be validated through Monte Carlo simulations.

To demonstrate an automated navigation analysis for rendezvous trajectories at L2, three trajectories are designed and analyzed that satisfy safety requirements, facilitate piloting, and limit propellant usage. For each trajectory, the navigation requirements are derived, followed by an optimal selection of sensors to fulfill the requirements.

REFERENCE FRAMES AND HALO ORBITS

Three frames of reference are pictured in Figure 1. The non-rotating inertial frame quantifies absolute reference states, such as the inertial position and velocity of the vehicles and celestial bodies. The origin is located at the center of the Earth, and the X_{ECI}-Y_{ECI} plane is defined by the J2000 equatorial plane.

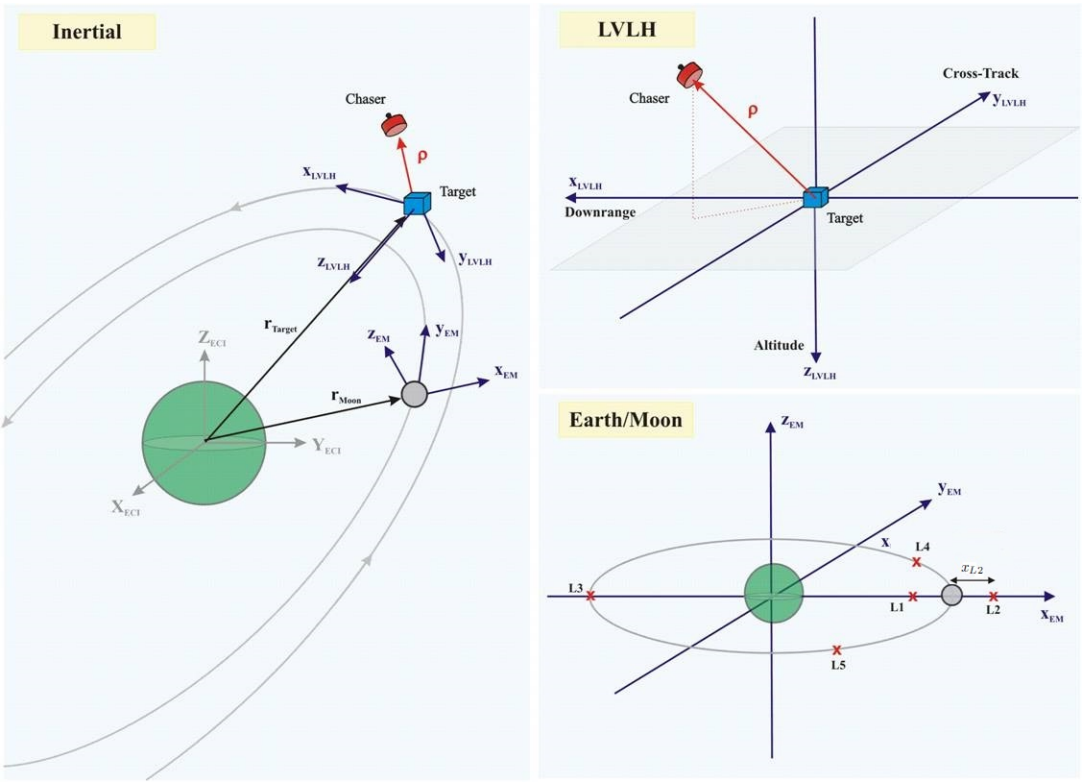

Figure 1: The Inertial, Earth/Moon Rotating and LVLH Reference Frames

Displayed on the top-right, the local vertical, local horizontal (LVLH) reference frame has its origin placed at the target vehicle. The x-axis is known as downrange, and is designated as the V-bar. The z-axis, or R-bar,

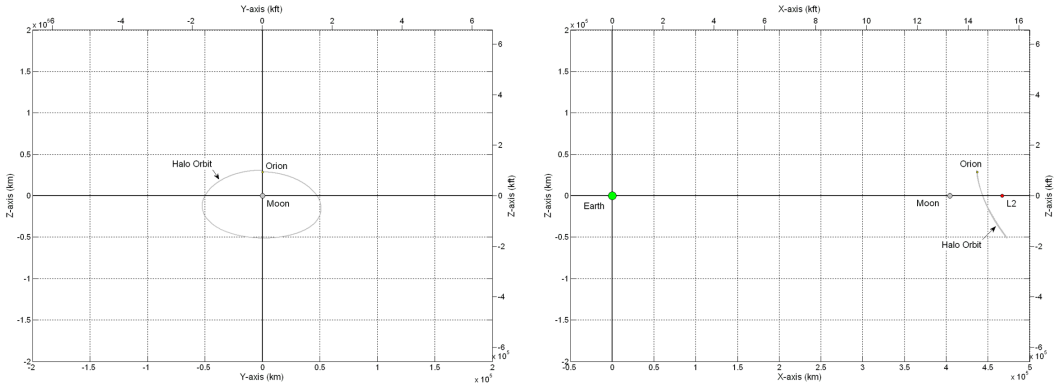

Figure 2: The Halo Orbit

is the altitude, describing the radial direction pointing towards the Earth or central body. Cross-track, is the y-axis or H-bar.

On the bottom right is the Earth/Moon rotating pulsating frame. Here, x_{EM} is pointed from the Earth to the Moon, z_{EM} is perpendicular to the plane of the Moon's orbit, and y_{EM} completes the triad pointing in the velocity of the Moon. The frame is pulsating because the distance between the Earth and the Moon is normalized to the same value, regardless of position of the Moon on its elliptical path. This frame of reference is used to display the halo orbits around L2. Data gathered from one such 14 day halo orbit is shown in Figure 2. This serves as the initialization point of the target vehicle, and can be maintained with minimal station-keeping maneuvers. The left view represents the trajectory as viewed from Earth looking towards the Moon. The right view is along the axis towards the Moon, within the same plane as the Moon's orbit.

TARGETING ALGORITHMS AT L2

Navigation requirements are directly affected by the targeting algorithms chosen. Targeting algorithms that are currently implemented for rendezvous in LEO or GEO are not necessarily applicable at L2. Therefore, a linear targeting algorithm, L2 Linearized Relative (LR) targeting, is created and utilized. If the relative equations of motion can be linearized to the state space representation form of

$$\dot{\mathbf{x}} = \mathbf{A} \cdot \mathbf{x}, \tag{1}$$

where $\mathbf{A}$ is the system matrix and $\mathbf{x}$ is the relative state, then the state transition matrix can be solved using the equation[12]

$$\Phi(\Delta t) = e^{\mathbf{A}\Delta t}, \tag{2}$$

where Δt is the transfer time. The state transition matrix can then be used to solve for the initial velocity required to target a desired position given a specified transfer time. The desired $\Delta\mathbf{v}$ can be determined by taking the difference between the vehicle's required velocity and its current velocity.

In the doctoral dissertation *Nonlinear Control Design Techniques for Precision Formation Flying at Lagrange Points*[10] by Luquette, the equations of motion at any Lagrange point are linearized for two spacecraft using the variables displayed in Figure 3. In the LVLH frame used here, the state space representation is:

$$\dot{\mathbf{x}} = \begin{bmatrix} 0 & \mathbf{I}_3 \\ \{\mathbf{\Xi}(t) - [n\times][n\times]\} & -2[n\times] \end{bmatrix} \cdot \mathbf{x} = \mathbf{A}_{LR} \cdot \mathbf{x}, \tag{3}$$

where $[n\times]$ is the cross product matrix of the orbital angular rate of the LVLH frame with respect to the barycenter of the two masses computed as

$$n = \left| (\mathbf{r}_{target} \times \mathbf{v}_{target}) / \left| \mathbf{r}_{target} \right|^2 \right|, \tag{4}$$

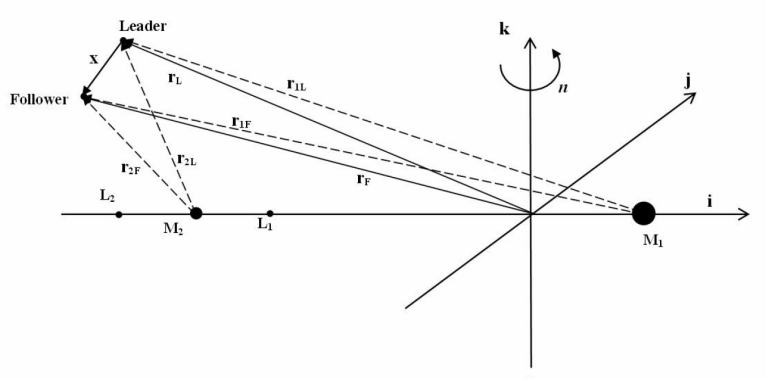

Figure 3: Variables for L2 Linearized Relative Targeting, in a Rotating Reference Frame[10]

and $\mathbf{\Xi}(t)$ equals

$$\mathbf{\Xi}(t) = -\left(\frac{\mu_1}{|\mathbf{r}_{1L}|^3} + \frac{\mu_2}{|\mathbf{r}_{2L}|^3}\right)\mathbf{I}_3 + \frac{3\mu_1}{|\mathbf{r}_{1L}|^3}[\mathbf{e}_{1L}\cdot\mathbf{e}_{1L}^\top] + \frac{3\mu_2}{|\mathbf{r}_{2L}|^3}[\mathbf{e}_{2L}\cdot\mathbf{e}_{2L}^\top]. \tag{5}$$

If the location of the Earth-Moon barycenter is approximated as the center of the Earth, then n is equal to the instantaneous orbital angular velocityy, as shown in Equation (4). Also, $\mathbf{r}_{1L}$ and $\mathbf{r}_{2L}$ are the vectors in the LVLH reference frame from the Earth and the Moon, respectively, to the target, and $\mathbf{e}_{1L}$ and $\mathbf{e}_{2L}$ are the unit vectors of $\mathbf{r}_{1L}$ and $\mathbf{r}_{2L}$. The constant μ_1 equals the gravitational parameter for the Earth, while μ_2 is the same parameter for the Moon.

LR targeting should be applicable for proximity operations at any trajectory within the restricted three-body problem, and was found to be accurate over both large transfer time and distances. Targeting points up to 30 km away with a one hour transfer time, the targeting errors were within 0.01%. For eight hour transfer times, the targeting errors were within 0.2%.

PRELIMINARY TRAJECTORY DESIGN

Three preliminary trajectories are developed and used to demonstrate the automated process of deriving navigation requirements and sensor suites for close proximity operations at L2. The include 1) the Double Co-Elliptic (DC), 2) the Line-of-Sight Corridor (LoS-C), and 3) the Line-of-Sight Glide (LoS-G). The Line-of-Sight Corridor and the Line-of-Sight Glide both take advantage of the near rectilinear motion of the chaser at L2.

For on-orbit operations, safety becomes a high priority to protect critical assets and crew members. In regards to rendezvous trajectories, the chaser vehicle must not enter particular *safety regions* or *constraint regions* surrounding the target until permission is granted, including free-drifts and dispersions. For example, all commercial vehicles visiting the ISS must receive an 'authority-to-proceed' prior to entering the 2 km by 1 km Approach Ellipsoid (AE) or the 200 m radius Keep Out Sphere (KOS).[13] Assuming similar safety constraints are adopted at L2 for future NASA missions, the three proposed trajectory designs conform to this safety requirement.

Double Co-Elliptic For the Orion program, NASA adopted the Double Co-Elliptic trajectory for rendezvous and docking in LEO. To preserve the same concept of operations and time-line procedures for close proximity at L2 as in LEO, the first proposed trajectory is a modified Double Co-Elliptic. Astronauts who have become familiar with piloting the DC will already be familiar with the positions and angles of the target relative to the chaser, as well as the time between maneuvers. Using the same trajectory for both environments

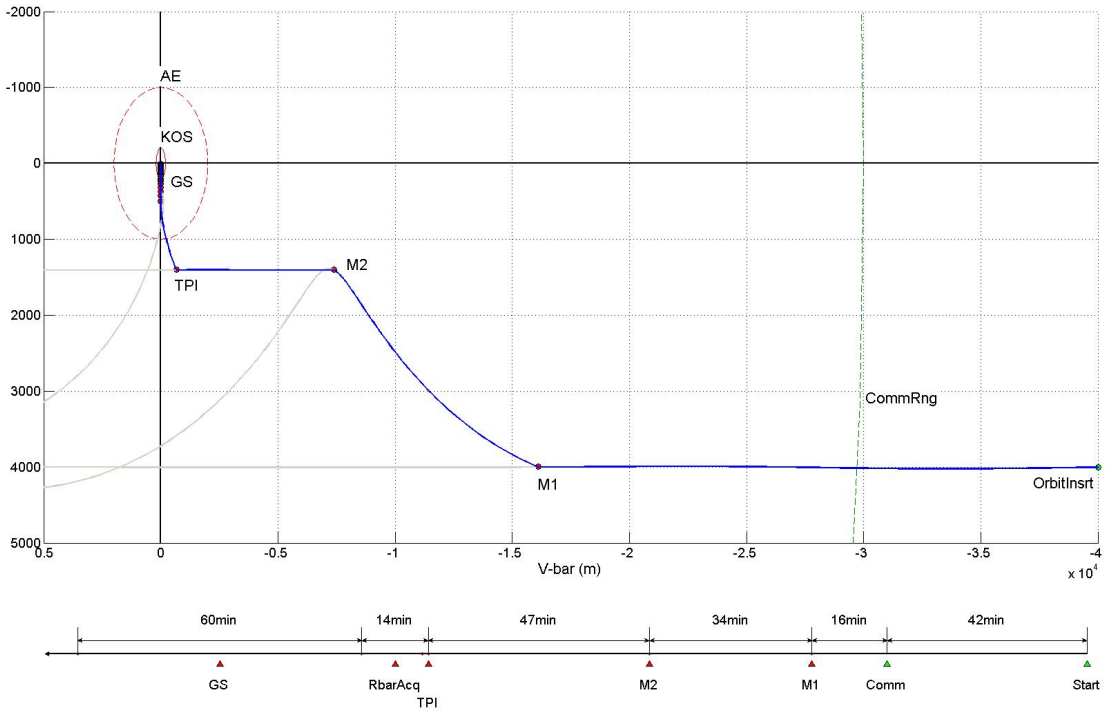

Figure 4: Double Co-Elliptic Trajectory with Free-Drifts in LEO. Nominal is in blue and free-drifts in grey.

can potentially save on training costs and reduce potential user error. For LEO, the Orion capsule would approach the target on two different co-elliptic altitudes causing the trajectory to be known as the Double Co-Elliptic,[14] and is shown in Figure 4. The chaser drifts along the 1.4 km co-elliptic until permission is granted to perform the Terminal Phase Initiation (TPI) maneuver that causes it to enter the AE. Docking is completed using a sequence of glideslope maneuvers (GS) that gradually brings the chaser to the target.[15]

When attempting to adapt a similar trajectory to L2, similar positions and times for maneuvers are used, but for the chaser to arrive at the target within a similar time frame, the trajectory cannot rely on traveling on a pure co-elliptic path. Since the approach rate on a co-elliptic trajectory is proportional to the relative altitude and the orbital angular rate, at L2 a vehicle on a true co-elliptic trajectory travels over 400 times slower than an equivalent profile in LEO. Instead, a pseudo co-elliptic trajectory is generated using LR targeting where the approach rates comparable to those in LEO are replicated.

The nominal trajectory at L2, with free-drifts, is shown in Figure 5. Both M1 and M2 maneuvers are still executed within communication range. The M3 point behaves as the TPI maneuver that sets the chaser to the *docking diamond*, a strategy used for all the L2 trajectories presented in this study, and displayed on the top-right of Figure 5. By approaching the docking axis at a $45°$ angle, the chaser nominally approaches no closer than 350 m to the target, which provides a margin from the 200 m KOS.

In this scenario, the positive V-bar is the docking axis. The M4 maneuver then acts as a correction maneuver, while the Hold Point maneuver, HP1, acquires and maintains the docking axis at 500 m downrange. After acquiring the docking axis, docking is again completed using the glideslope (GLS1) maneuvers.

Line-of-Sight Corridor

At L2, the relative dynamics support the possibility of approaching the target directly along the docking port. It is possible to keep the chaser within a given field-of-view of the target until entering the docking

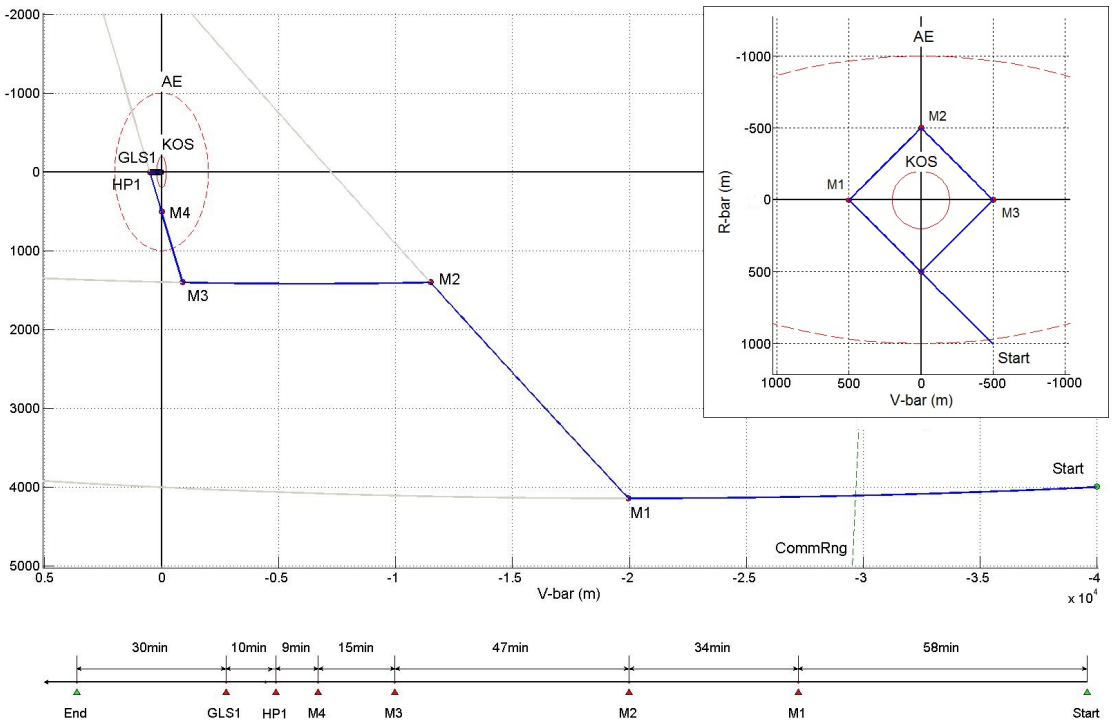

Figure 5: Double Co-Elliptic Trajectory at L2, with Free-Drifts, Time-Line and the Docking Diamond.

diamond, allowing it to use sensors with a restricted field-of-view, or use reflectors on the target that are only visible within a restricted field-of-view, defined from the docking axis. This type of trajectory could facilitate the use of angles-only navigation, by constantly and predictably changing the bearing of the target to the chaser. To ensure it still possesses sufficient safety characteristics, the target is never approached directly, but instead between a set of user defined angles.

In total, the Line-of-Sight Corridor trajectory is defined by four angles: an approach angle, θ; two trigger angles, α and β; as well as an offset angle less than either trigger angle, $\phi < \alpha$ and $\phi < \beta$. The trigger and offset angles are illustrated in Figure 6. This strategy assumes that the chaser approaches the target a small distance below and parallel to the docking axis, which can be rotated from the positive x-axis of the LVLH frame by the approach angle, θ. For simplicity of demonstration, the approach angle is set to zero, and is not shown in this paper.

The chaser travels parallel to the docking axis until it reaches the first trigger angle, α, defined counter-clockwise from the docking axis. The chaser uses a series of burns perpendicular to the x-axis in order to rotate the velocity vector a total of $(\alpha + \phi)$ counterclockwise or $(\beta + \phi)$ clockwise, in order to stay within the approach corridor of angle $(\alpha + \beta)$. This process continues until reaching the desired range. At all times, with possible exception of the rendezvous initiation conditions which are previously determined as safe, the chaser never approaches the target at any angle closer than ϕ.

Assuming rectilinear motion, these maneuvers create a series of similar triangles. An application of the law of sines and mathematical induction allows one to solve for the nth targeting point as

$$\mathbf{r}_f(n) = \left\{ \begin{array}{ll} A_n \left[\begin{array}{ccc} cos(\beta) & 0 & -sin(\beta) \end{array} \right]^\intercal & if\ n\ is\ odd \\ A_n \left[\begin{array}{ccc} cos(\alpha) & 0 & sin(\alpha) \end{array} \right]^\intercal & if\ n\ is\ even \end{array} \right\} = \left[\begin{array}{ccc} x_n & y_n & z_n \end{array} \right]^\intercal, \qquad (6)$$

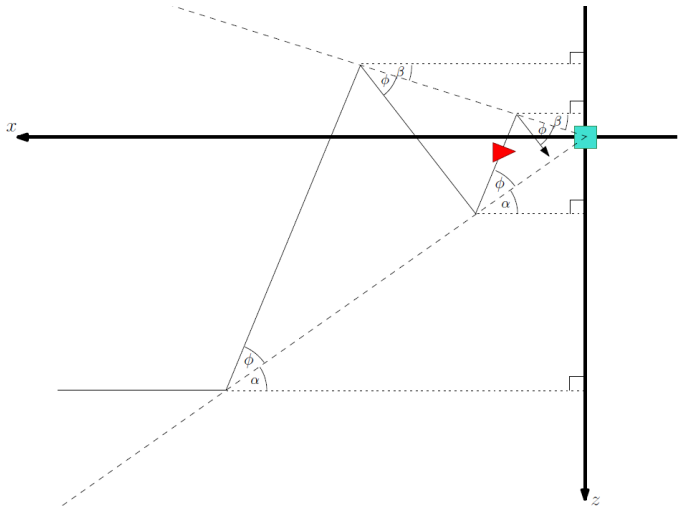

Figure 6: Derivation of the Line-of-Sight Corridor. The chaser arrives at either trigger angle, and the resulting rotation in a tilted target axis frame is displayed.

where

$$A_n = A_0 \left[\frac{sin(\phi)}{sin(\alpha + \beta + \phi)} \right]^n, \tag{7}$$

and A_0 is the range that the chaser first arrives at the corridor. In order to keep the downrange velocity component constant, for the purpose of conserving fuel, the transfer time is proportional to the distance traveled downrange. That is,

$$\Delta t_n = \frac{\Delta x_n \cdot T_{corridor}}{\Delta X_{corridor}} = \left\{ \begin{array}{ll} \frac{B_n \cdot cos(\alpha+\phi) \cdot T_{corridor}}{\Delta X} & if\ n\ is\ odd \\ \frac{B_n \cdot cos(\beta+\phi) \cdot T_{corridor}}{\Delta X_{corridor}} & if\ n\ is\ even \end{array} \right\}, \tag{8}$$

where

$$B_n = A_0 \left[\frac{sin(\beta + \alpha)}{sin(\phi)} \right] \left[\frac{sin(\phi)}{sin(\alpha + \beta + \phi)} \right]^n, \tag{9}$$

and $T_{corridor}$ is the total time traveled within the corridor, with the total downrange distance $\Delta X_{corridor}$.

For the specific trajectory analyzed in this paper, the *symmetric approach* is used, where $\beta = \alpha$, and is shown in Figure 7. The trajectory starts 4 km below and 50 km ahead of the target, with an initial speed to reach the z-axis in approximately 3 hours, a downrange velocity of -4.63 m/s. Here, $\alpha = \beta = 10°$, and $\phi = 7.5°$. These values allow the first maneuver, M1, to be taken inside radar range, and still be able to safely avoid the approach ellipsoid at any approach angle θ. M2 acts as the TPI maneuver, entering the AE while avoiding the KOS. The chaser drifts to the M3 point, where it is set to the docking diamond. After this, all further maneuvers are similar to the DC trajectory.

Line-of-Sight Glide

Similar to the Line-of-Sight Corridor, the Line-of-Sight Glide assumes rectilinear motion to allow the chaser to approach with the target always within sight, but safely between a trigger angle and an offset angle. However, in a further effort to save fuel, the offset angle is not set across the line-of-sight between the chaser and the target, but on the same side as the trigger angle. Although this increases the number of maneuvers, the Δv required per maneuver is drastically reduced.

The Line-of-Sight Glide is defined by three angles: an approach angle, θ, a trigger angle, α, and an offset angle, $\phi < \alpha$. Unlike the LoS-C, β is the angle of rotation, determined to be $(\alpha - \phi)$. This can be seen in Figure 8. The approach angle can be defined as earlier; for this scenario it is still set to zero. The chaser

approaches the target a small distance below and parallel to the x-axis, until it reaches the trigger angle, α, now defined as the angle between the velocity vector and position vector of the chaser. However, instead of rotating $(\alpha + \phi)$, it rotates $(\alpha - \phi) = \beta$ counter-clockwise, and continues on. The chaser continues to move on this segment, until it hits the trigger angle α, and rotates β, and repeats this until it reaches the desired range.

These maneuvers create one set of similar triangles, each of which rotates depending on the step number, n. The nth targeting point is

$$\mathbf{r}_f(n) = A_n \begin{bmatrix} cos(\alpha + n\beta) & 0 & sin(\alpha + n\beta) \end{bmatrix}^\mathsf{T} = \begin{bmatrix} x_n & y_n & z_n \end{bmatrix}^\mathsf{T}, \tag{10}$$

where

$$A_n = A_0 \left[\frac{sin(\phi)}{sin(\alpha)}\right]^n = A_0 \left[\frac{sin(\alpha - \beta)}{sin(\alpha)}\right]^n, \tag{11}$$

and A_0 is the range that the chaser first reaches the trigger angle.

For this paper, the rotational angle of $\beta = 5°$ with a nine step glide was chosen to allow for a sizable amount of maneuvers to correct free-drifts, without unnecessarily increasing the maneuver count. If $z_0 = 4000$ m, the trigger angle to land directly on the docking diamond after the glide was determined to be $\alpha = 20.551°$. Using these values, the trajectory shown in Figure 9 is constructed. M1 is a correction maneuver once inside

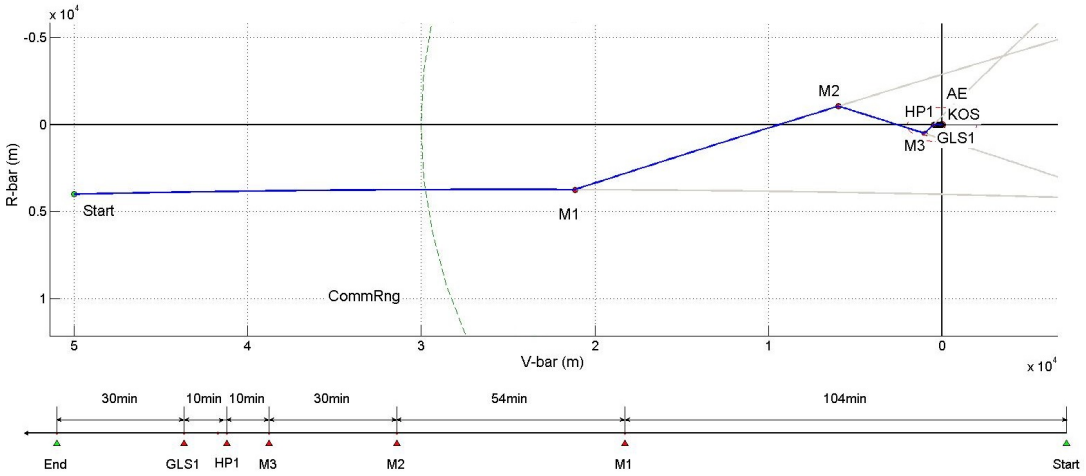

Figure 7: The Line-of-Sight Corridor Trajectory

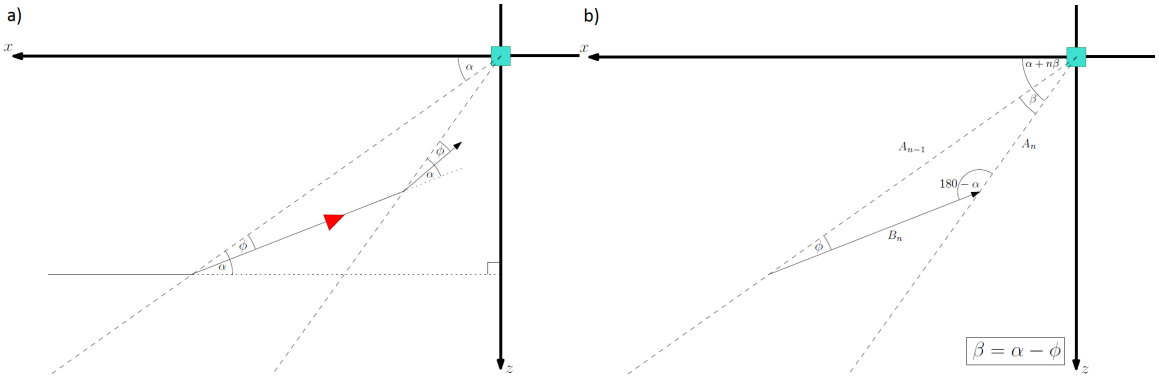

Figure 8: Derivation of the Line-of-Sight Glide. The left image (a) displays the chaser arriving at the trigger angle, and the resulting rotation. The right image (b) displays the similar triangles made by step n.

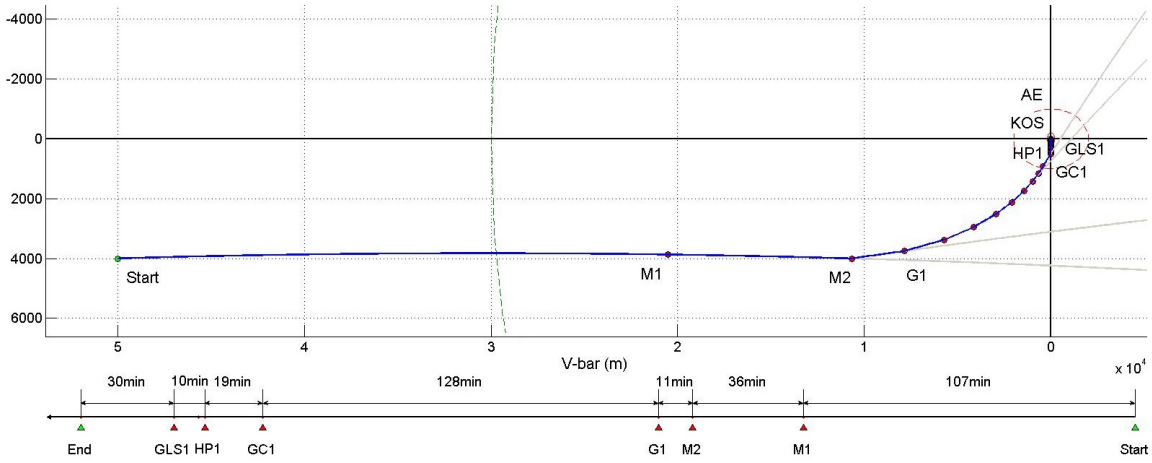

Figure 9: The Line-of-Sight Glide Trajectory

communication range, while GC1 is a correction maneuver after the LoS maneuvers are completed and the spacecraft is drifting on the docking diamond to the z-axis. Either M2 or G1 can act as the TPI maneuver.

To minimize Δv, all maneuvers after M2 strictly decrease the approach rate, which must be neutralized by the HP1 maneuver regardless. This requires the transfer times to be proportional to the altitude traveled per maneuver, or

$$\Delta t_n = \frac{\Delta z_n \cdot T_{glide}}{\Delta Z_{glide}} = \frac{B_n \cdot sin(n\beta) \cdot T_{glide}}{\Delta Z_{glide}}, \tag{12}$$

where

$$B_n = A_0 \left[\frac{sin(\beta)}{sin(\phi)}\right] \left[\frac{sin(\phi)}{sin(\alpha)}\right]^n, \tag{13}$$

and T_{glide} is the total time to travel the altitude ΔZ_{glide} on the glide.

Trajectory Summary Table 1 summarizes the maneuvers performed for the Double Co-Elliptic, Line-of-Sight Corridor and the Line-of-Sight Glide. The maximum Δv for each scenario, along with the total number of impulsive maneuvers, is included. The Double Co-Elliptic takes the shortest time, has the lowest maximum Δv and the closest TPI maneuver. The Line-of-Sight Corridor has the fewest maneuvers, while the Line-of-Sight Glide has the lowest fuel usage. All trajectories were designed with a focus for ease of piloting, either through a heritage concept of operations or constant angle triggers.

Table 1: Nominal Trajectory Comparison

Trajectory	Time (hours)	Max Δv (m/s)	Total Δv (m/s)	Maneuvers	Range of TPI (km)
DC	3.38	2.94	8.84	4	1.664
LoS-C	3.96	3.03	9.36	3	6.072
LoS-G	5.67	2.13	6.00	11	8.702 to 11.395

STOCHASTIC CONSIDERATIONS

With the trajectory designs complete in a deterministic sense, random aspects of the system are now considered. Trajectory dispersions throughout the duration of the profile are directly caused by sources such as

the initial trajectory dispersions at the start of proximity operations, imperfect thrusters, modeling errors, and disturbance accelerations. In this study, the error distributions for each of these sources are fixed according to the pre-determined value for each scenario.

The trajectory dispersions caused by these parameters can be counteracted by determining the type, quality, and quantity of sensors the spacecraft is using, or the spacecraft's *sensor suite*. Ultimately, the top level mission requirements specifying constraints on the trajectory dispersions indirectly determines how accurately the position and velocity must be known by the navigation system. By combining an accurate navigation system with targeting maneuvers developed in the previous sections, dispersions can be contained.

The cost and mass of higher quality and quantity of sensors must be factored against the improved performance to find an optimal sensor suite. To capitalize on the speed of linear covariance analysis and the robustness of Monte Carlo analysis, this research employs both techniques to evaluate the effects of stochastic processes on the trajectory design. This study uses LinCov simulations for solving the required accuracy of the sensor suite, and Monte Carlo for verification.

The basic techniques used in this section and the sensor suite analysis discussion are introduced by David Woffinden and Louis Breger in *Automated Derivation and Verification Requirements for On-Orbit Rendezvous*[16]. For the derivation and detailed explanation of these techniques in full, please refer to this article.

STOCHASTIC NAVIGATION, SENSITIVITY, AND REQUIREMENT DERIVATION OVERVIEW

Instead of fully incorporating sensor models and filter algorithms to capture the effects of the navigation system, it is perhaps useful to directly perturb the true states by an error bound representative of the anticipated navigation performance. This concept is called *stochastic navigation*, and it is central to the derivation of navigation requirements. In this context, the navigation state is modeled as the true state plus a bounded error, denoted as $\delta\bar{\mathbf{e}}$. Then,

$$\hat{\mathbf{x}} = \mathbf{x} + \delta\bar{\mathbf{e}}. \tag{14}$$

Stochastic navigation can be implemented within both Monte Carlo and LinCov simulations, as demonstrated by Woffinden and Breger.[16]

With stochastic navigation, the navigation error can be scaled to determine the navigation error bound, and ultimately the navigation requirements. Given the linear nature of the covariance operations, linear superposition can be applied to the variance of any element of the true state.[17,16] The variance of the total dispersion, σ_p^2, can be expressed as

$$\sigma_p^2 = \sum_{i=1}^{n} \sigma_{p|\delta_i}^2. \tag{15}$$

For the ensuing developments, the performance index p designates the total relative trajectory dispersions. With this equation, the effects different levels of navigation error have on the trajectory dispersions can be quickly observed without having to do an additional simulation run. Using sensitivity analysis, the total dispersion can be derived from the root-sum-square of the individual sources at any point along the trajectory.

So the navigation requirements can be derived by scaling the navigation error by the coefficient, α_i^2, until the resulting trajectory dispersions $\sigma_{p^*}^2$ reach a maximum value and violate a specified safety condition. Once this maximum value is identified, it corresponds to the maximum allowable navigation requirement for that particular region.

$$\sigma_{p^*}^2 = \sum_{i=1}^{n} \alpha_i^2 \sigma_{p|\delta_i}^2. \tag{16}$$

In this application, only one source is scaled: the navigation error based upon the relevant *navigation region* which corresponds to the times of key maneuvers. This coefficient is solved through a bi-sectional search, such that the 3-σ dispersions of the trajectory do not intersect with a pre-determined safety region but come within a specified tolerance.

An example of this can be seen for the M1 maneuver of the Double Co-Elliptic trajectory in Figure 10. The scaling factor, α, corresponds to the navigation requirement at the maneuver. The blue ellipses represent

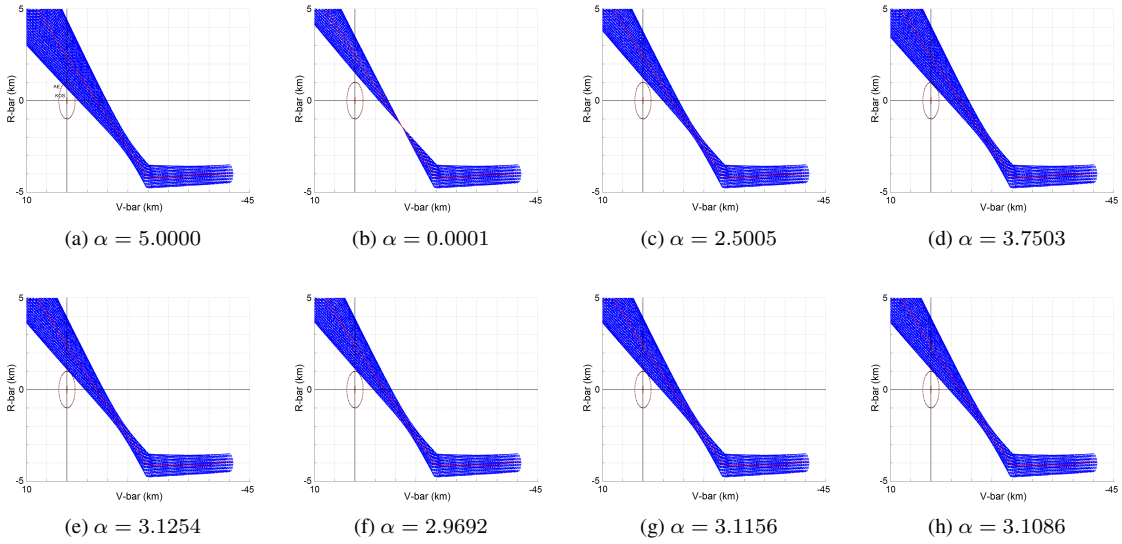

(a) $\alpha = 5.0000$ (b) $\alpha = 0.0001$ (c) $\alpha = 2.5005$ (d) $\alpha = 3.7503$

(e) $\alpha = 3.1254$ (f) $\alpha = 2.9692$ (g) $\alpha = 3.1156$ (h) $\alpha = 3.1086$

Figure 10: Eight Steps of Requirement Derivation through Bi-Sectional Search

the 3-σ trajectory dispersions that result from the current scaling factor. Each step of the scaling sequence below is completed in a fraction of a second. The derivation of the navigation requirements scales a default stochastic navigation 3-σ error of 50 m and 0.057 m/s in downrange, cross-track, and altitude.

REQUIREMENT DERIVATION RESULTS AND VERIFICATION

The navigation requirements are derived for each time interval, or navigation region, of all three trajectories. The DC requirements are shown in full for each free-drift, while the LoS-C and LoS-G are summarized. Not all maneuvers define a navigation region, but every maneuver satisfies the free drift safety requirements using the navigation error derived for the specified region.

Double Co-Elliptic Navigation Requirements Before the hold point, all maneuvers for the DC trajectory determine a navigation region. For each maneuver, a figure is displayed. All figures contain three sub-figures. Sub-figure (a) displays the final scaling value of the automated requirement derivation and predicted trajectory dispersions. The resulting derived navigation requirement is subsequently implemented within simulations as a stochastic navigation error. Sub-figure (b) demonstrates the implementation in both the LinCov and Monte Carlo simulations. Each grey line is the navigation error for an individual Monte Carlo run, with the sampled 3-σ bound displayed in black. The navigation error for a single Monte Carlo run is highlighted, to demonstrate how it is correlated in time. The maroon colored 3-σ bound represents the simulated navigation error in LinCov.

Finally, the validation of the derived navigation results is completed by comparing the trajectory dispersions of the Monte Carlo simulation to the dispersions predicted by LinCov. Sub-figure (c) shows the trajectory dispersions resulting from the scaled navigation requirements. Each grey line is an individual Monte Carlo run, and the sampled 3-σ ellipses are displayed in black. The red ellipses show the 3-σ bounds predicted from LinCov. For a two dimensional, 3-σ ellipse, 98.9% of the samples are expected to be contained. If linear covariance properly predicts dispersions, rounding to the nearest integer, no more than 3 Monte Carlo runs are expected to lie outside of either ellipse.

The first navigation region of the double co-elliptic trajectory contains the M1 maneuver. Before the TPI maneuver, the Approach Ellipsoid (AE) is used as the constraint region. From Figure 11a, it is seen that a

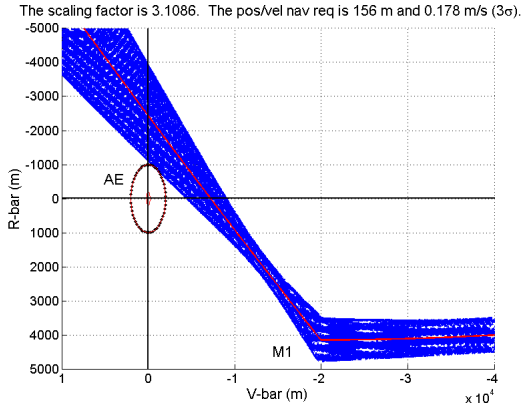

(a) Requirement Analysis with the Approach Ellipsoid

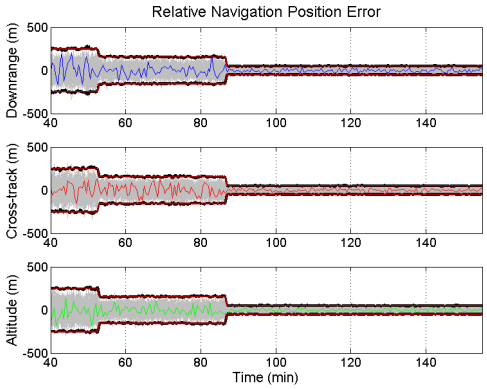

(b) Relative Position LVLH 3-σ Errors

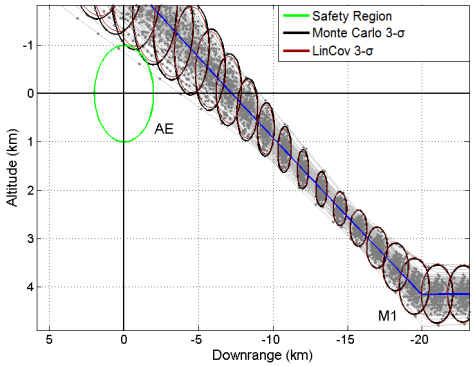

(c) LinCov and 250 Monte Carlo Runs

Figure 11: M1 Free-Drift Trajectory of the Double Co-Elliptic

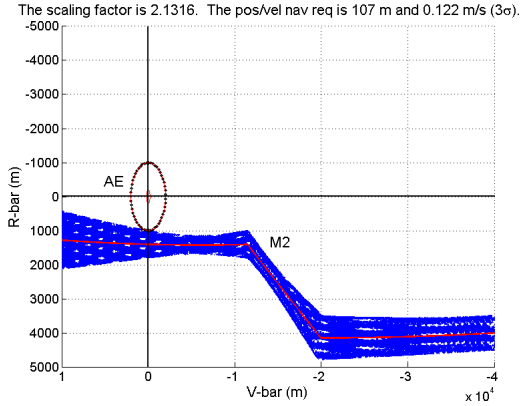

(a) Requirement Analysis with the Approach Ellipsoid

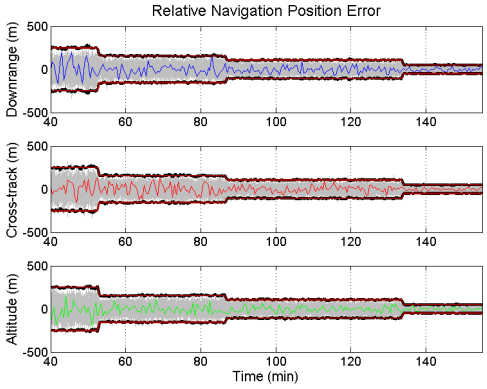

(b) Relative Position LVLH 3-σ Errors

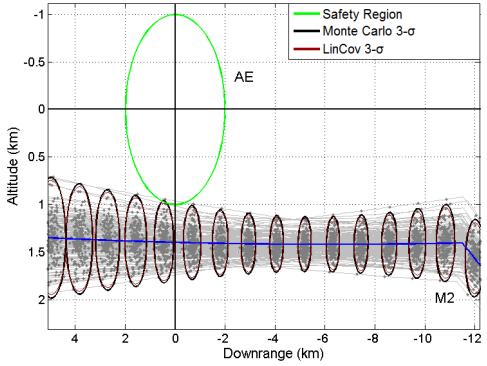

(c) LinCov and 250 Monte Carlo Runs

Figure 12: M2 Free-Drift Trajectory of the Double Co-Elliptic

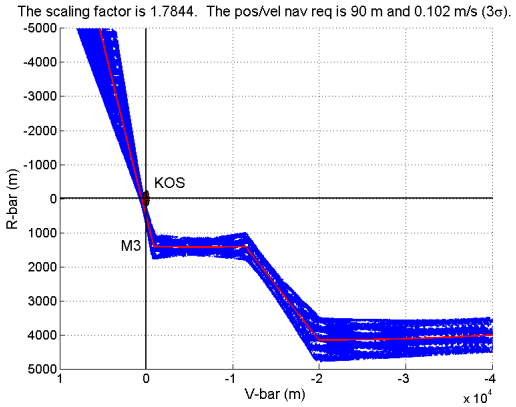

(a) Requirement Analysis with the Keep Out Sphere

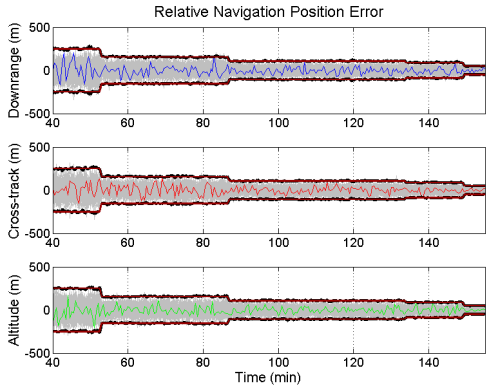

(b) Relative Position LVLH 3-σ Errors

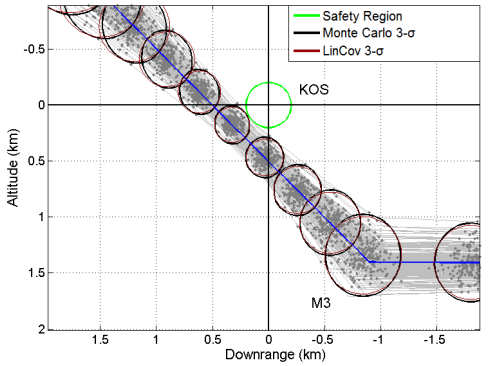

(c) LinCov and 250 Monte Carlo Runs

Figure 13: M3 Free-Drift Trajectory of the Double Co-Elliptic

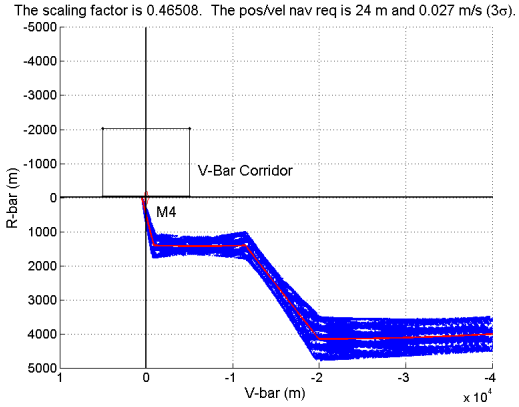

(a) Requirement Analysis with the Extended V-Bar Corridor

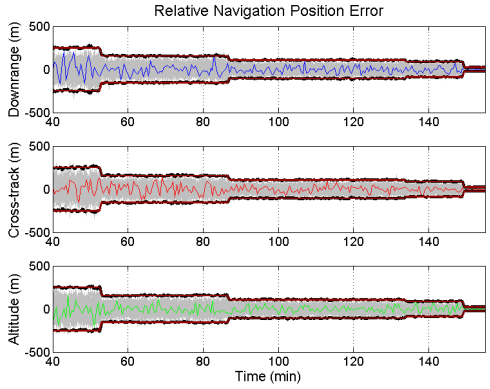

(b) Relative Position LVLH 3-σ Errors

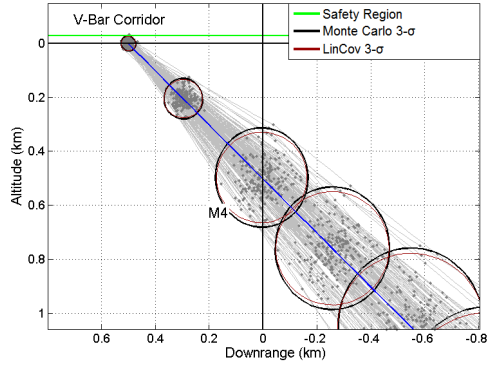

(c) LinCov and 250 Monte Carlo Runs

Figure 14: M4 Free-Drift Trajectory of the Double Co-Elliptic

Region	Maneuvers	Start (min)	Safety	Scaling	Pos. 3-σ (m)	Vel. 3-σ (m/s)
1	M1	53.0	AE	3.1086	155.43	0.177
2	M2	87.0	AE	2.1316	106.58	0.122
3	M3	134.0	KOS	1.7844	89.220	0.102
4	M4 to Dock	149.4	V-bar Corr.	0.4651	23.254	0.027

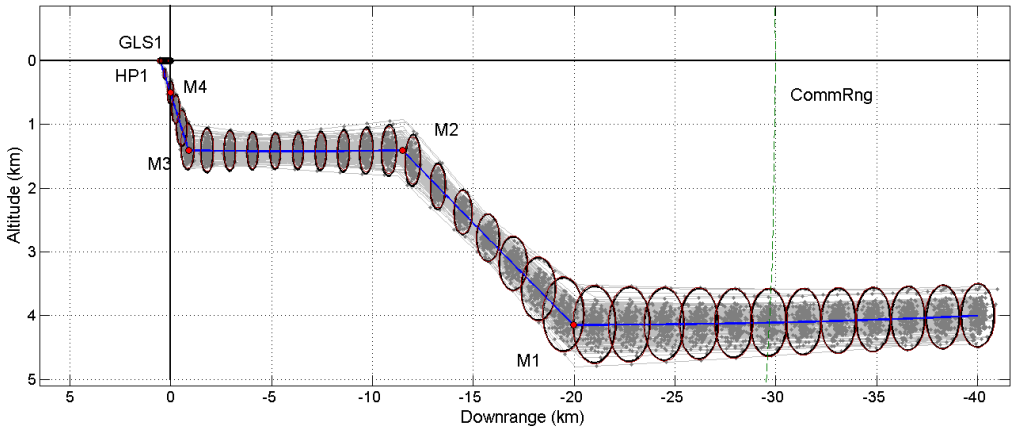

Figure 15: Linear Covariance Analysis, Monte Carlo, and Summary Table for the Double Co-Elliptic

3-σ navigation requirement of 156 m, corresponding to a scaling factor of 3.1086, ensures the M1 free-drifts do not enter the AE.

To begin validating this derived navigation requirement, it is first implemented as the stochastic navigation error for the first navigation region in the Monte Carlo simulation as shown in Figure 11b, from the 53rd to 87th minute. The 3-σ navigation error bounds generated from 250 Monte Carlo samples (black) overlays the derived navigation requirement (red). The individual errors for each run (grey) are seen to approximate white noise. Figure 11c compares the LinCov to Monte Carlo trajectory dispersions due to the derived navigation requirement associated with the 3-σ navigation requirement of 156 m. Of the 250 Monte Carlo runs, 3 lie outside of the LinCov 3-σ ellipse near the AE, as expected.

The navigation errors for the preceding maneuver are then used to determine the navigation errors for the following maneuvers. The navigation requirements for the M2 maneuver are also derived to refrain from entering the AE, as shown in Figure 12a. The derived 3-σ navigation requirement for the second navigation region is 107 m. Figure 12b shows this derived value implemented in the Monte Carlo simulation starting from the 87th minute to the 134th minute. Figure 12c shows that both the Monte Carlo and LinCov predictions share a consistent result that the safety condition is satisfied.

Figure 13 demonstrates the final scaling for the third phase of the trajectory starting with the M3 maneuver. M3 acts as the TPI maneuver, and the M3 free-drift is shown to be safe with respect to the Keep Out Sphere (KOS) with a 3-σ navigation requirement of 90 m. No Monte Carlo run lies outside of the LinCov 3-σ ellipse at the KOS in Figure 13c.

M4 is a pre-docking correction maneuver, and an extended approach corridor acts as a constraint region to restrict dispersions at this time. The V-bar corridor extends a 16° opening in the KOS along the docking axis to the holding point 500 m away from the target. This can be seen in Figure 14a and 14c. A 3-σ navigation requirement of 24 m is required for the M4 maneuver, as shown in Figure 14a, and completes the final navigation region in Figure 14b. By combining the derived navigation requirements for each trajectory segment as developed in Figures 11 through 14, the complete end-to-end rendezvous navigation requirements

Region	Maneuvers	Start (min)	Safety	Scaling	Pos. 3-σ (m)	Vel. 3-σ (m/s)
1	M1	99.0	AS	2.7101	135.51	0.154
2*	M2	152.7	KOS	4.4566	222.83	0.254
3	M3 to Dock	182.7	V-bar Corr.	0.4510	22.552	0.0257

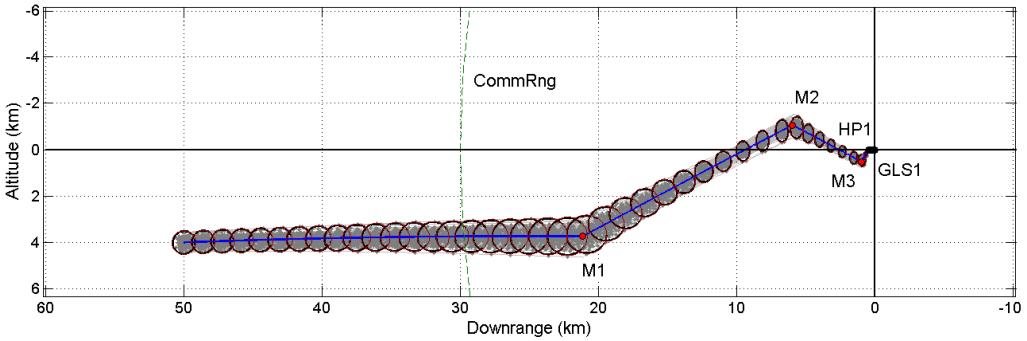

Figure 16: Completed Linear Covariance Analysis, Monte Carlo, and Summary Table for LoS-Corridor. *The second navigation region is set to the values of the first for determination of the third, as well as the end-to-end trajectory analysis.

and trajectory dispersions predicted from these requirements are shown in Figure 15.

Line-of-Sight Corridor Navigation Requirements In order to allow the LoS trajectories to be capable of docking at any approach angle, a 2 km radius Approach Sphere (AS) is used as the constraint region where the AE otherwise would. For the LoS-Corridor, the AS is only used to derive navigation requirements for the M1 maneuver. The M2 maneuver uses the KOS to derive requirements. The M3 navigation requirements are determined with respect to the V-bar Corridor, which aligns the target to dock.

The summary table and full trajectory comparison for the LoS-Corridor can be seen in Figure 16. For the navigation requirements for the LoS-Corridor trajectory, the required navigation scaling did not, at first, decrease as range decreased. This resulted in excessively large dispersions inside the AS. Instead, the scaling values of the first navigation region were also used for the second, and it will be seen that this does not reduce the number of sensor suites that satisfy the navigation requirements for this trajectory.

The low number of maneuvers for this trajectory decreased the amount of navigation regions required, but the LoS-C M3 point is more than 600 m farther than the DC M4 point, yet required approximately the same navigation requirement. The LoS-Corridor will require higher quality sensors during the close-range segment of the rendezvous.

Line-of-Sight Glide Navigation Requirements For the LoS-Glide, because of the high amount of maneuvers, not every maneuver has a corresponding navigation region. Instead, the allowable navigation errors for the full navigation region is equal to the minimum of the allowable navigation error of the individual maneuvers contained within it. In the case of the LoS-Glide, the minimum occurs at the last maneuver within the navigation region. It is these last, key maneuvers that are analyzed.

As was the case with the LoS-Corridor, the AS is used in place of the AE to allow for any approach angle. The first navigation region contains M1 and M2, which share the AS safety region, as G1 acts as the TPI maneuver. The remaining glide maneuvers, G1 through G8, are not allowed to free-drift into the KOS. These maneuvers are further split into two navigation regions expected to have similar navigation accuracy: those

Region	Maneuvers	Start (min)	Safety	Scaling	Pos. 3-σ (m)	Vel. 3-σ (m/s)
1	M1 and M2	101.9	AS	2.3989	119.95	0.137
2	G1 through G6	148.7	KOS	1.1607	58.035	0.0662
3	G7 and G8	253.5	KOS	0.5109	25.543	0.0291
4	GC1 to Dock	276.3	R-bar Corr.	0.3412	17.060	0.0194

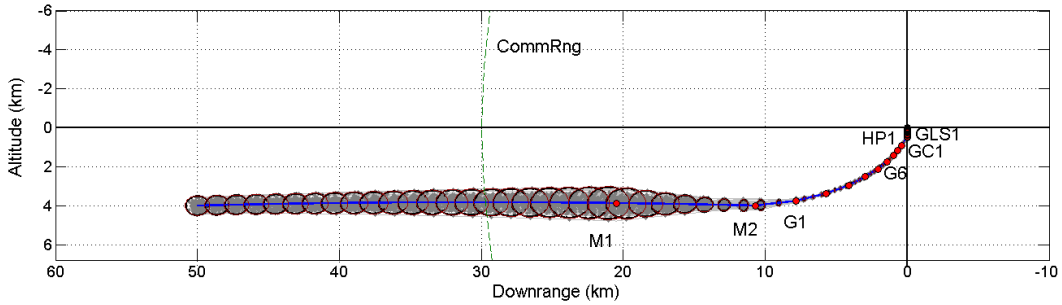

Figure 17: Completed Linear Covariance Analysis, Monte Carlo, and Summary Table for LoS-Glide

inside and outside of a 2 km range, the expected operational range of a lidar. The navigation requirements for the second navigation region, containing G1 through G6, are determined from the G6 free-drift. Similarly, the third navigation region contains only G7 and G8, with the navigation requirement determined from the G8 free-drift. The fourth and final navigation region is determined so that the correction maneuver, GC1, does not leave an R-bar extended approach corridor.

The navigation requirements for the LoS-Glide were more restrictive than the previous trajectories, as can be seen in the summary table of Figure 17. Although at farther range the LoS-Glide has comparable requirements, the mid-range G6 maneuver required a 3-σ navigation requirement of 58.0 m to avoid the KOS. This is a requirement that is not matched by the LoS-Corridor or the Double Co-Elliptic until their final navigation regions, preparing for docking. At close-range, the navigation requirements narrowed further. The last maneuvers of the glide required a 3-σ navigation requirement of 25.5 m, while the final correction maneuver required 17.1 m.

Overall, for both the LoS trajectories, no LinCov 3-σ ellipses entered any of the safety regions, demonstrating the effectiveness of the automated approach of deriving navigation requirements. This was validated by the Monte Carlo runs, as no Monte Carlo run drifted through any safety regions for all of the maneuvers analyzed. All LinCov 3-σ ellipses match well with their Monte Carlo counterparts.

SENSOR SUITE ANALYSIS

After determining the navigation requirements for all trajectories, a sensor suite analysis can be conducted. The sensor suite analysis considers a full combination of available sensors, and simulates how each would affect the navigation states throughout an entire trajectory, by determining the navigation error that would occur from that specific combination. This is completed using linear covariance analysis.

The navigation performance resulting from each sensor suite is then compared to the navigation requirements found through the requirement derivation. A sensor suite satisfies all requirements if the navigation accuracy provided is greater than the allowable navigation error for all navigation regions. This can be seen visually in Figure 18. If the color corresponding to a certain sensor suite is above the black constant values representing the navigation requirements, for any time duration in any graph, the sensor suite fails.

In this study, five sensors available at L2 are analyzed: a lidar, an optical sensor, a target based ground up-

dated available at rendezvous initiation, a chaser based ground update also available at rendezvous initiation, and an RF (radio frequency) sensor.

The sensors have different accuracies dependent on the level of quality chosen. It is anticipated that ground updates of the target and chaser vehicles will be required to initialize the onboard navigation filter. To represent the different quality of ground updates that may be experienced, three options are investigated. However, sensor suites are considered having no lidar, RF sensor, or optical sensor, giving a total of four options for three sensors. In total, there are 576 possible sensor combinations. The sensors considered ensure that all typical measurements types are provided, yet are unique and dissimilar.

The sensors will also be weighted, for the spacecraft's limiting factors such as monetary cost or physical mass, so that an optimal sensor suite can be selected from all passable combinations. For ease of demonstration, in this study high quality, medium quality, or low quality sensors are given weights of three, two, or one, respectively. If a particular sensor is not used, it is given a weight of zero.

Double Co-Elliptic Sensor Suites The results of the DC sensor suite analysis can be seen in Figure 18. The constant black lines represent the derived navigation requirements from Figure 15. For the Double Co-Elliptic, 255 of the 576 sensor suites satisfied the navigation requirements. Of those, the lowest weighted are shown in Table 2. The ground updates are abbreviated as ITGU for initial target ground update and ICGU for initial chaser ground update. For the individual sensors, a low quality sensor is represented as (L), medium as (M), and high as (H). If the sensor was not included within a suite, it is indicated by (N).

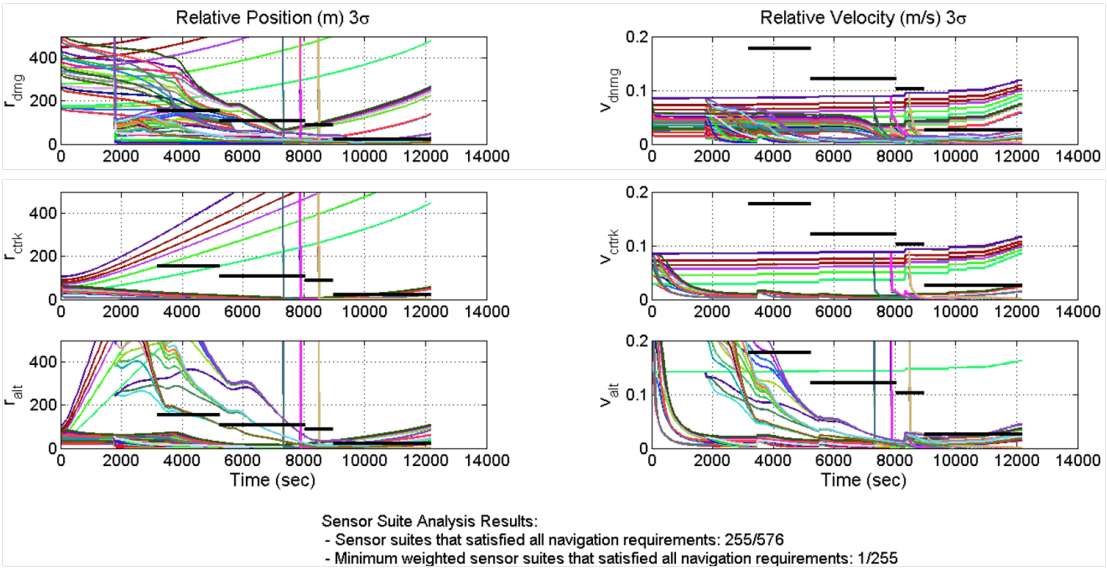

Figure 18: The Double Co-Elliptic Sensor Suite Analysis Results

The DC trajectory did not require as accurate of a navigation state estimate as the other two trajectories presented. Consequently, a full suite of low quality sensors fulfilled all the requirements. Because measurement types were unique and dissimilar, every sensor provided a different role in the navigation system, and all had to be active to fulfill the full navigation requirements with a sensor suite of low overall weight.

Table 2: Optimal Sensor Suites for the Double Co-Elliptic

Sensor Suite ID	Weight/Cost	ITGU	ICGU	Optical Sensor	Lidar	RF Sensor
555	5	L	L	L	L	L

Line-of-Sight Corridor Sensor Suites The results of the LoS-Corridor sensor suite analysis are shown in Figure 19, with 234 suites satisfying all requirements. Although there are only two navigation regions, many suites failed the second. The second region corresponds to the M3 maneuver, which required higher navigation accuracy at a range of 1.12 km from the target. As a result, a full suite of low quality sensors did not satisfy all navigation requirements.

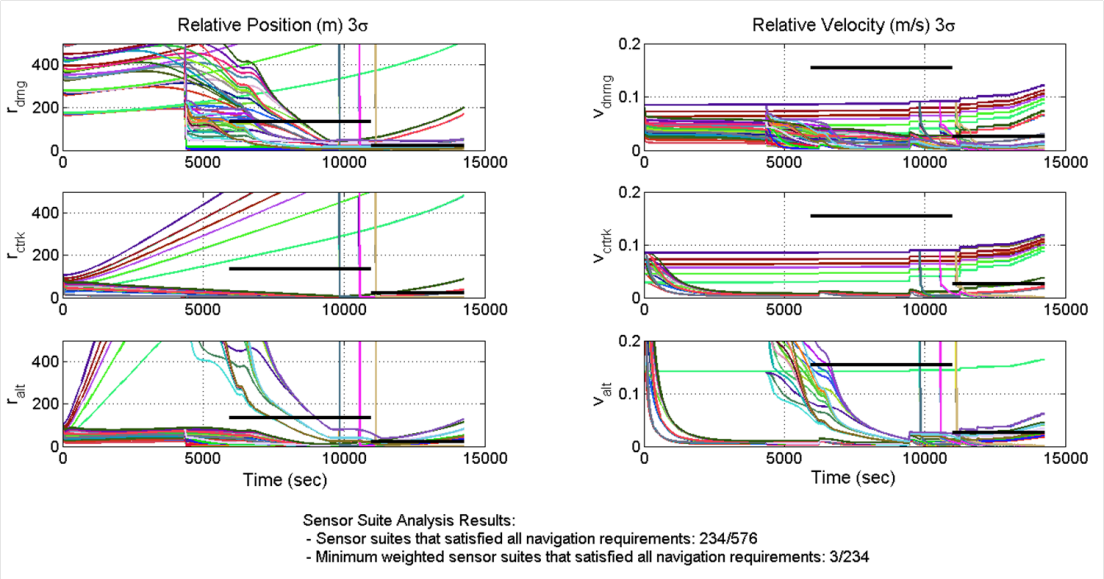

Figure 19: The LoS-Corridor Sensor Suite Analysis Results

The lowest weighted sensor suite that satisfied all navigation requirements are shown in Table 3. Three sensor suite combinations that satisfy the navigation requirements with the a total weight of 6. Similar to the DC analysis results, all sensors were necessary to fulfill requirements with an overall low sensor suite weight. The optimal three selections also required a medium quality lidar, RF ranging sensor, or optical camera. The advantages of an improved ground update only benefited navigation accuracy at farther ranges, and did not have any effect on whether a low weight suite passed or failed.

Table 3: Optimal Sensor Suites for the LoS-Corridor

Sensor Suite ID	Weight/Cost	ITGU	ICGU	Optical Sensor	Lidar	RF Sensor
539	6	L	L	M	L	L
551	6	L	L	L	M	L
554	6	L	L	L	L	M

Line-of-Sight Glide Sensor Suites Figure 20 contains the results of the LoS-Glide sensor suite analysis. For the LoS-Glide, 207 of the 576 satisfied the requirements. The LoS-Glide had the strictest navigation requirements at close-range, and this is reflected in the total number of suites that passed all navigation requirements.

The lowest weighted sensor suites are shown in Table 4. Only non-trivial suites, where no individual sensor could be reduced in quality and still satisfy the navigation requirements, are shown. Similar to the LoS Corridor, the lowest sensor suite weight is 6. Only one suite of this weight passed, which required a medium quality lidar for the final two glide maneuvers. However, with the extended optical sensor operational range

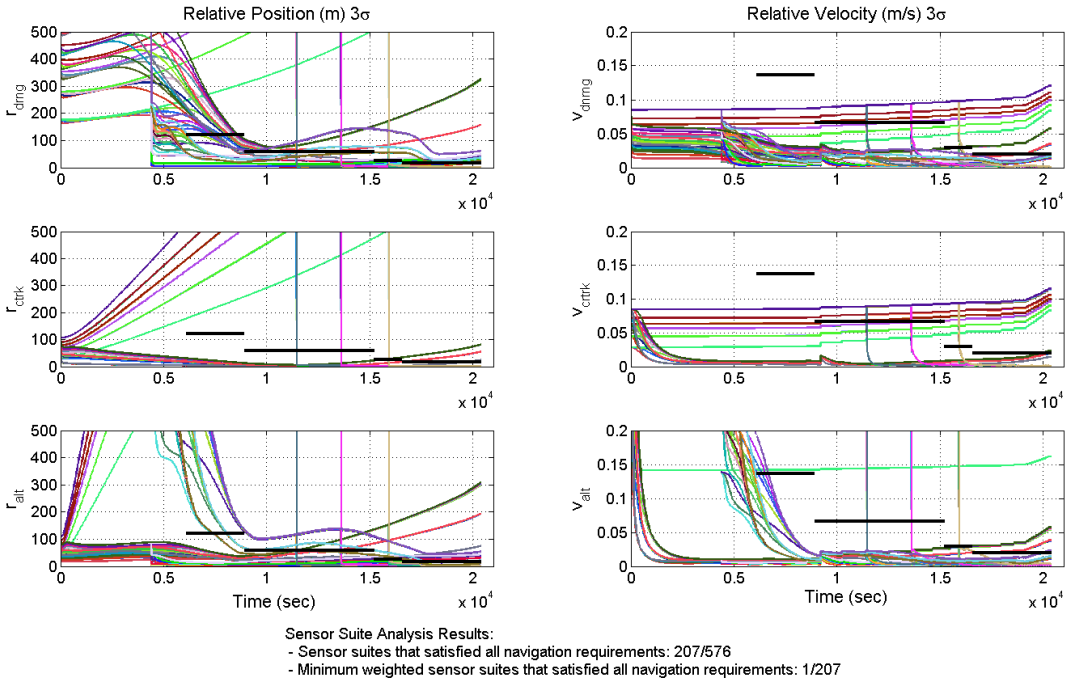

Figure 20: The LoS-Glide Sensor Suite Analysis Results

at medium quality, the close-range requirements can also be fulfilled with the use of a medium quality optical sensor and RF-sensor. If the weights were significantly different and a medium quality lidar was found to be cost ineffective, this would be a viable option.

Table 4: Optimal Sensor Suites for the LoS-Glide

Sensor Suite ID	Weight/Cost	ITGU	ICGU	Optical Sensor	Lidar	RF Sensor
551	6	L	L	L	M	L
538	7	L	L	M	L	M

CONCLUDING REMARKS

The Earth-Moon L2 Lagrange point is a potential deep-space destination for a space station or propellent depot. Possible reasons include its location in an Interplanetary Superhighway System, optimal environment for fuel storage, and ability to act as a radio quiet zone or communications satellite to the far side of the Moon. However, for the Earth-Moon L2 point to fulfill this potential, rendezvous capabilities between a target vehicle in a halo orbit around L2 and a chaser must be developed. Several trajectories and navigation systems currently used for rendezvous at LEO or other destinations with comparable relative motion dynamics cannot be directly applied.

Utilizing L2 Linearized Relative targeting within an L2 local vertical, local horizontal frame of reference, three preliminary trajectories were developed: the L2 Double Co-Elliptic, the LoS-Corridor, and the LoS-Glide. Although the Double Co-Elliptic trajectory does not exhibit all of the benefits it has in LEO, adapting it for L2 was possible and did not incur excessive fuel usage, while preserving the concept of operations for all pilots and systems. The LoS-Corridor and LoS-Glide utilized the rectilinear motion at L2 to create trajectories with recognizable trigger angles and offset angles for safety. The LoS-Corridor can act within the

bounds of sensors or reflectors constrained with limited field-of-views, while the LoS-Glide minimizes fuel consumption required to arrive at the target.

To ensure the trajectory design is robust to potential contingency scenarios, free-drift trajectories associated with each maneuver are required to remain outside predesignated safety regions. To determine the navigation requirements, stochastic navigation was implemented to both Monte Carlo and LinCov simulations. Sensitivity analysis concepts then provided a mechanism to create an automated requirement derivation capability. By deriving requirements for relevant navigation regions, that corresponded to key maneuvers and constraint regions, navigation requirements for an entire rendezvous trajectory were determined.

For L2 and other potential deep space missions where many design parameters are in flux and undetermined, having the capability to efficiently derive navigation requirements in an automated and reliable fashion becomes a valuable asset. This paper demonstrated the process of quickly deriving navigation requirements for three trajectories and then validated the results. The navigation requirements were also contrasted versus the navigation performances of 576 different sensor suites. This capability to translate top level mission design requirements into lower level navigation performance parameters can assist future exploration programs by providing rapid analysis tools during the preliminary trajectory design phase.

REFERENCES

[1] M. Lo and S. Ross, "The Lunar L2 Gateway: Portal to the Stars and Beyond," *AIAA Space 2001 Conference*, vol. A01-40254, 28 - 30 August, 2001. Albuquerque, New Mexico.

[2] F. Zegler and B. Kutter, "Evolving to a Depot-Based Space Transportation Architecture," *AIAA SPACE Conference & Exposition*, vol. 2010-8638, 30 August - 2 September 2010. Anaheim, California.

[3] M. Bobskill, et al., "Earth-Moon L1/L2 Infrastructure - What Role Does It Play?," *Human Exploration Community Workshop on the Global Exploration Roadmap*, 14 - 16 November 2011. San Diego, California.

[4] P. D. Merritt, "Continuous Communications For The Lunar Farside: How Do We Get There? A Differentially Corrected Halo Transfer Orbit," *AIAA Meeting Papers on Disc*, vol. 96-0016, 15 - 18 January 1996. Reno, Nevada.

[5] T. N. Edelbaum, "Libration Point Rendezvous," *Analytical Mechanics Associates (Journal)*, vol. N70-26184, February, 1970.

[6] R. B. Gerding, "Rendezvous Equations in the Vicinity of the Second Libration Point," *Journal of Spacecraft and Rockets*, vol. 8, No. 3, pp. 292 – 294, 1970.

[7] G. Gomez, K. Howell, J. Masdemont and C. Simo, "Station-Keeping Strategies for Translunar Libration Point Orbits," *American Astronomical Society (Journal)*, vol. AAS 98-168, 1998.

[8] R. Serban, et al., "Halo Orbit Mission Correction Maneuvers Using Optimal Control," March 31st, 2001.

[9] A. B. Jenkin and E. T. Campbell, "Generic Halo Orbit Insertion and Dispersion Error Analysis," *Astrodynamics Specialist Conference and Exhibit*, vol. 2002-4527, 5-8 August 2002. Monterey, California.

[10] R. J. Luquette, *Nonlinear Control Design Techniques for Precision Formation Flying at Lagrange Points*. PhD thesis, University of Maryland, November 21st, 2006.

[11] W. Fehse, *Automated Rendezvous and Docking of Spacecraft*. Cambridge Aerospace Series, Cambridge University Press, New York, December 22nd, 2003.

[12] F. Golnaraghi and B. C. Kuo, *Automatic Control Systems, 9th Edition*. John Wiley & Sons, New Jersey, 2010.

[13] "International Space Station (ISS) to Commercial Orbital Transporation Services (COTS) Interface Requiements Document (IRD)," *National Aeronautics and Space Administration - International Space Station Program*, vol. SSP 50808, Revision C, pp. 3–81, November 2011.

[14] C. D'Souza, et al., "Orion Rendezvous, Proximity Operations, and Docking Design and Analysis," *AIAA Guidance, Navigation, and Control Conference and Exhibit*, vol. 2007-6683, 20 - 23 August 2007. Hilton Head, South Carolina.

[15] F. D. Clark, P. T. Spehar, J. P. Brazzel, and H. D. Hinkel, "Laser-based Relative Navigation and Guidance for Space Shuttle Proximity Operations," *26th Annual AAS Guidance and Control Conference*, vol. 2003, 5-9 February Breckenridge, CO.

[16] D. Woffinden and L. Breger, "Automated Derivation and Verification of Requirements for On-Orbit Rendezvous," *AIAA Guidance, Navigation, and Control Conference*, vol. 2013-4964, 19 - 22 August 2013. Boston, Massachusetts.

[17] P. Maybeck, *Stochastic Models, Estimation, and Control: Volume 1*. Academic Press, New York, 1979.